




RESEARCH PAPER



## Perturbation of mRNP biogenesis reveals a dynamic landscape of the Rrp6-dependent surveillance machinery trafficking along the yeast genome

Kévin Moreau <sup>a</sup>, Aurélia Le Dantec <sup>a</sup>, Christine Mosrin-Huaman<sup>a</sup>, Yves Bigot <sup>b</sup>, Benoit Piégu<sup>b</sup>, and A. Rachid Rahmouni<sup>a</sup>

<sup>a</sup>Centre de Biophysique Moléculaire, UPR 4301 du CNRS, Orléans, France; <sup>b</sup>Physiologie de la Reproduction et des Comportements, UMR 7247 INRA-CNRS, Nouzilly, France

### ABSTRACT

Eukaryotic cells have evolved a nuclear quality control (QC) system to monitor the co-transcriptional mRNA processing and packaging reactions that lead to the formation of export-competent ribonucleoprotein particles (mRNPs). Aberrant mRNPs that fail to pass the QC steps are retained in the nucleus and eliminated by the exonuclease activity of Rrp6. It is still unclear how the surveillance system is precisely coordinated both physically and functionally with the transcription machinery to detect the faulty events that may arise at each step of transcript elongation and mRNP formation. To dissect the QC mechanism, we previously implemented a powerful assay based on global perturbation of mRNP biogenesis in yeast by the bacterial Rho helicase. By monitoring model genes, we have shown that the QC process is coordinated by Nrd1, a component of the NNS complex (Nrd1-Nab3-Sen1) involved in termination, processing and decay of ncRNAs which is recruited by the CTD of RNAP II. Here, we have extended our investigations by analyzing the QC behaviour over the whole yeast genome. We performed high-throughput RNA sequencing (RNA-seq) to survey a large collection of mRNPs whose biogenesis is affected by Rho action and which can be rescued upon Rrp6 depletion. This genome-wide perspective was extended by generating high-resolution binding landscapes (ChIP-seq) of QC components along the yeast chromosomes before and after perturbation of mRNP biogenesis. Our results show that perturbation of mRNP biogenesis redistributes the QC components over the genome with a significant hijacking of Nrd1 and Nab3 from genomic loci producing ncRNAs to Rho-affected protein-coding genes, triggering termination and processing defects of ncRNAs.

### ARTICLE HISTORY

Received 6 February 2019  
Revised 6 March 2019  
Accepted 6 March 2019

### KEYWORDS

mRNP biogenesis; mRNP quality control; yeast; RNA-seq; ChIP-seq

### Introduction

Expression of protein-coding genes in eukaryotic cells is a multistep process in which the genetic message is transcribed from DNA into a pre-mRNA molecule that undergoes several modification reactions such as 5'-end capping, splicing, 3'-end cleavage and polyadenylation while being assembled into a ribonucleoprotein particle (mRNP) that will be exported into the cytoplasm for translation. The current view is that the nascent transcript emerging from the transcription complex is sequentially loaded with a variety of protein factors that ensure its integrity and mediate its maturation and transport from the site of transcription to the nuclear pore for export [1,2]. Like most complex biological activities, the process of co-transcriptional mRNP biogenesis is error-prone and thus, cells have evolved a surveillance system that detects malformed mRNPs resulting from inappropriate or inefficient processing and packaging reactions [3,4]. Aberrant mRNPs that fail to pass the quality control (QC) steps are targeted for destruction by the RNA degradation machinery associated with the nuclear exosome complex [5,6]. The interdependence and coordination between transcript synthesis and the other activities of mRNP biogenesis, QC and nuclear export are facilitated by the C-terminal domain (CTD) of the largest subunit of RNA polymerase II (RNAP II) that serves as a platform for sequential recruitment of the various acting factors.

Although the real frequency of mRNP biogenesis defects occurring under physiological context is actually unknown, its putative prevalence does not allow a direct study of the QC mechanism within the cellular framework. Thus, most insights into the QC process have come from studies focusing on yeast *S. cerevisiae* mutants with defects in the THO-Sub2 complex that mediates mRNP assembly and export. It was shown that the mechanism of nuclear retention and degradation of defective mRNPs depends on the presence of the nucleus-specific exosome-associated exonuclease Rrp6 as well as components of the exosome activating complex TRAMP (Trf4-Air2-Mtr4). However, these analyses which relied on depletion or mutation of specific components of the THO-Sub2 complex were unable to provide an integrated and functional view of the QC system, especially regarding the co-transcriptional recognition of aberrancies and its role in the subsequent triggering of mRNA decay. Moreover, the observed effects were limited mostly to a subset of transcripts produced under heat shock conditions such as HSP104 [7–9].

In recent years, we implemented an experimental approach in which the general perturbation of mRNP biogenesis in *S. cerevisiae* by the RNA-dependent helicase/translocase activity of the bacterial Rho factor generates sufficient amounts of defective mRNPs as substrates to investigate the QC process (reviewed in [10]). Our analyses of a set of model mRNAs such as PMA1 substantiated the key role of the 3'-5' exonuclease Rrp6

in the elimination of defective mRNPs [11–13]. Furthermore, the results revealed that the QC process is coordinated by Nrd1, a component of the early termination complex (Nrd1-Nab3-Sen 1) which is recruited by the CTD of RNAP II through its CTD-interacting domain (CID). The targeting and degradation of Rho-induced aberrant PMA1 mRNA is associated with a large increase of Nrd1 recruitment to the transcription complex with a concomitant enrichment of Rrp6 together with its cofactor Rrp47 as well as components of the TRAMP complex [11,13].

In the present work, we sought to investigate the general nature of the previous observations by analyzing the mRNA QC activities over the whole yeast genome. We performed high-throughput RNA sequencing (RNA-seq) to survey a broad collection of mRNPs whose biogenesis is affected by Rho action. Among the 1,015 transcripts that showed decreased levels in the presence of Rho, almost a half (491 transcripts) were rescued to nearly their original levels by the depletion of Rrp6. This genome-wide perspective was extended by generating high-resolution maps (ChIP-seq) of the distribution of most QC components along the yeast chromosomes before and after perturbation of mRNA biogenesis by Rho. Our results show that the perturbation of mRNA biogenesis redistributes the binding of QC components over the genome with a large shift of Nrd1 and Nab3 from gene loci producing non-coding RNAs (ncRNAs) prone to processing and decay (CUTs, SUTs and snoRNAs) to protein-coding genes. Nrd1 and Nab3 are apparently titrated out from ncRNAs genomic features by a large recruitment to Rho-affected mRNA gene loci, leading to transcriptional termination defects of ncRNAs. The ChIP profiles display statistically significant overlapping of occupancy peaks suggesting a co-localization of the QC components over discrete portions of the Rho-affected mRNA genes.

## Results

### Rho-based perturbation of mRNA biogenesis in yeast

In our experimental approach, large amounts of defective mRNPs can be generated by the activity of bacterial Rho factor in yeast cells to serve as substrates to study the QC mechanism (reviewed in [10]). Rho expressed from a centromeric plasmid under the control of the Doxycycline (Doxy) repressible TetO7 promoter is directed to the nucleus by a nuclear localization signal fused to the C-terminus of the protein. Rho is a hexameric helicase/translocase that binds to naked, C-rich and preferentially unstructured portions of RNA. This binding activates the ATPase activity of the protein leading to its translocation along the RNA chain in a 5' to 3' direction. Our previous investigations with a model gene (*PMA1*) showed that Rho action along the nascent transcript interferes with the normal recruitment of mRNA processing and packaging factors yielding mRNPs that are recognized as defective and eliminated by the QC apparatus in a process involving the 3'-5' exonuclease activity of Rrp6. By monitoring the rescue of the *PMA1* mRNA level in different deletion strains, we showed that the targeting and degradation of Rho-induced aberrant mRNPs by Rrp6 is stimulated by the cofactors Rrp47 and Mpp6 as well as the TRAMP complex [13]. An interesting finding made in those studies, which was also reported by others [14–16], is that Rrp47 plays an important role in a mutual protein stabilization with Rrp6, highlighting a close physical association between the two

protein partners [16]. In effect, removal of one partner by gene deletion induces a depletion of the other partner by more than 90% [13]. Given that the *rrp6Δ* strain is known to be temperature sensitive and to have a slow growth as well as a slight genetic instability, we used in the present work the *rrp47Δ* strain to deplete Rrp6 when needed for the rescue of the Rho-affected transcripts.

### High throughput determination of Rho-induced aberrant mRNPs targeted by the Rrp6-dependent QC

To survey the effect of Rho on a large collection of mRNAs, we performed stranded RNA-seq using rRNA-depleted RNAs isolated from wild-type and *rrp47Δ* yeast cells grown in the presence (Rho-repressing conditions) or the absence (Rho-inducing conditions) of the effector, Doxy. For each condition, two biologically independent samples were used for libraries preparation and sequencing. In general, the results of the duplicates were highly correlated with Spearman correlation coefficients above 0.98 (Figure S1). The RNA-seq single reads were aligned on the *S. cerevisiae* genome and the mapped reads matching annotated transcripts were distributed into different RNA biotypes. About 60% of the mapped transcripts were protein-coding mRNAs and the remaining 40% represented ncRNAs including CUTs, SUTs, XUTs, snRNAs and snoRNAs (Figure S2A). Upon Rho expression in the wild-type cells, a substantial fraction of the transcripts within all RNA biotypes showed variations, either up or down, in their steady-state levels as illustrated by the scatter plots (Figure S2B).

We first focused our analyses on the Rho-induced variations in the abundance of mRNAs to have insights into the fate of defective mRNPs. We calculated the statistical significance of the variations (mRNA ratios between +Rho and -Rho conditions) and plotted the log<sub>2</sub> fold change of the level of each mRNA as a function of its log<sub>2</sub> mean expression (Figure 1A). Among the 5,132 mRNAs mapped with the RNA-seq results, 1,015 mRNAs showed decreased levels upon Rho expression in wild-type cells with a log<sub>2</sub> fold change  $\leq -0.5$  (blue dots in Figure 1A). A nearly symmetrical fraction of mRNAs had increased steady-state levels in the presence of Rho with a log<sub>2</sub> fold change above 0.5 (red dots in Figure 1A). The remaining part of mRNAs did not show statistically significant variations in the presence of Rho (grey dots). As expected, we interpret these results as an indication that Rho activity in yeast does not affect the biogenesis of all mRNPs. Indeed, all nascent transcripts may not proffer RNA segments suitable for Rho loading and activation. Alternatively, the Rho-induced higher levels observed for a fraction of mRNAs could be explained by a trans-regulation effect where the Rho-mediated reduction in the level of one mRNA or ncRNA up-regulates the expression of one or several transcripts. When the statistical significance calculations (ratios between +Rho and -Rho mRNA levels) and plotting were applied to the RNA-seq datasets of the mRNAs produced in the *rrp47Δ* strain, about half (491 transcripts) of the mRNAs that were diminished by Rho action in wild-type cells were partially reverted close to their normal levels by the deletion of the *RRP47* gene, i.e. depletion of Rrp6 (grey dots in Figure 1B). Four of these mRNAs were randomly picked for individual validation by RT-qPCR and

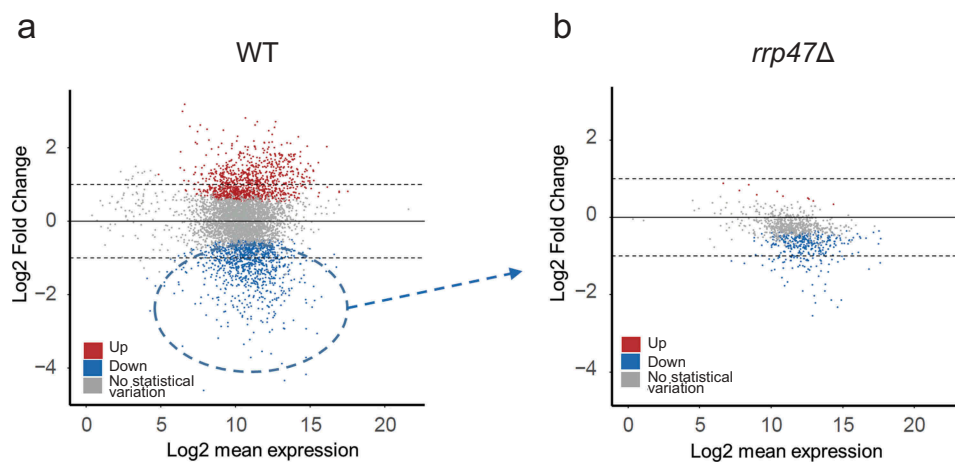


**Figure 1.** Fate of a subpopulation of mRNAs down-regulated by Rho action in Wt cells and their rescue in a strain with a deletion of *RRP47*, i.e. depleted of Rrp6. **a)** MAplot of the  $\log_2$ FoldChange ratios of the mRNAs between -Rho and + Rho conditions ( $\log_2(\pm Rho)$ ) from WT cells distinguishes three sub-populations: statistically upregulated in red, statistically downregulated in blue and no statistical variation in grey. The dashed blue circle surrounds the population of interest which is down-regulated. **b)** MAplot as in a but for the mRNAs obtained from *rrp47Δ* cells and focuses only on the subset of mRNAs that were down-regulated in WT cells as determined in a.

showed relative recoveries of their levels in the *rrp47Δ* strain (Figure S3). The remaining half of the Rho-mediated down-regulated mRNAs (524 transcripts) did not show any significant recovery in the *rrp47Δ* strain, according to our cut-off value (blue dots in Figure 1B).

To have a global view on these sorting results, we used the RNA-seq datasets obtained under the different conditions to generate averaged meta-transcript profiles (Figure 2). The profiles for the whole mapped mRNAs did not show any significant variations among the different conditions, reflecting the averaging of the RNA-seq raw data. For the whole group of down-regulated mRNAs (1,015 transcripts), the action of Rho in the wild-type cells leads to a general decrease in the intensity of the averaged meta-transcript, indicating that, on average, a fraction of corresponding mRNPs has

been recognized as aberrant and eliminated. This conclusion is supported by the absence of any marked effect of Rho on the level of the averaged profile for mRNAs produced in the *rrp47Δ* strain. Sorting the group of down-regulated mRNAs into two categories (rescued and non-rescued by Rrp6 depletion) showed two different trends regarding the Rho-induced variations as well as the shape of the averaged meta-transcript profiles. The pool of rescued mRNAs appears to contain relatively less expressed transcripts with a higher average reads coverage at the 5' end of the metagene which could be ascribed to the accumulation of short transcripts resulting from RNAP II pausing at the early part of the genes. Such paused transcription complexes are likely terminated by the action of Rho as reported previously [17] which could explain the absence of their full recovery in the *rrp47Δ* strain. The

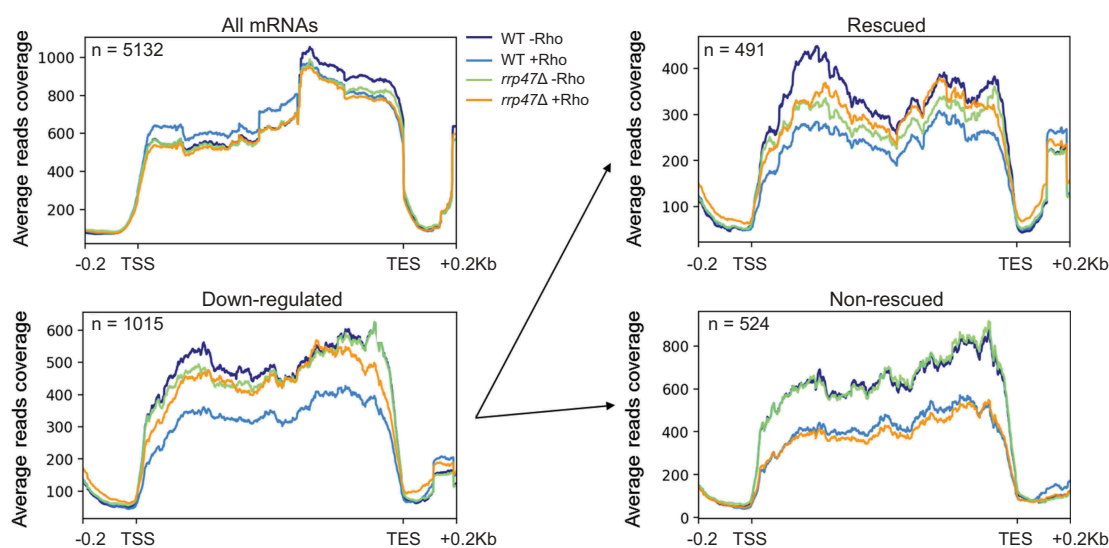


**Figure 2.** Meta-transcript profiles variations of mRNAs obtained from WT and *rrp47Δ* cells in the absence or presence of Rho. The top left graph shows the average reads coverage for all analyzed mRNAs. The bottom left graph represents the down-regulated mRNAs subpopulation as determined in Figure 1A. The two right graphs display the two groups of the down-regulated mRNAs sorted according to their rescue in the *rrp47Δ* genetic background (Rescued) or not (Non-rescued) as determined in Figure 1B. For all the graphs, the dark blue line represents mRNAs obtained from WT cells in the absence of Rho whereas the light blue gives the meta-profiles of the mRNAs obtained from the same cells but in the presence of Rho. Light green and orange display the meta-profiles of the mRNAs obtained from the *rrp47Δ* strain in the absence and presence of Rho, respectively.

meta-transcript profiles obtained with the pool of non-rescued mRNAs reveal an averaged higher expression of the transcripts with a clear absence of rescue in the *rrp47Δ* strain. We infer that the absence of recovery in the *rrp47Δ* strain for this mRNA group is likely an indication that the corresponding Rho-induced defective mRNPs are targeted by the alternative Rat1-dependent QC pathway, as we reported previously for HXK1 mRNP [18]. An in-depth comparative analysis between the two mRNA populations and their specific processing by the two QC pathways (Rrp6-dependent and Rat1-dependent) will be published elsewhere (Moreau et al. manuscript in preparation). Altogether, these results show that a set of at least 491 yeast mRNPs whose biogenesis was affected by Rho activity are recognized and targeted for destruction by the Rrp6-dependent QC machinery.

### Perturbation of mRNP biogenesis by Rho affects the *Nrd1*-dependent processing and termination of ncRNAs

To investigate further the response of Rrp6-dependent QC to Rho-mediated perturbation of the yeast transcriptome, we extended the comparative analyses of the RNA-seq datasets to ncRNAs including CUTs, SUTs and snoRNAs which are known to be degraded and/or processed by Rrp6 [19–21]. We generated averaged meta-transcript profiles for each ncRNA category produced in the absence or presence of Rho and in wild-type or *rrp47Δ* cells. In contrast to the Rho-induced decreasing trend observed for the affected mRNAs, the metaprofiles of the ncRNAs showed rather a slight but significant increase of the averaged steady-state levels in the presence of Rho. The Rho-induced stabilization of the ncRNAs is more pronounced in the *rrp47Δ* strain (Figure S4). This differential effect of Rho between mRNAs and ncRNAs is clearly illustrated when the ratios of RNA levels between +Rho and -Rho conditions are plotted as log<sub>2</sub> fold change values

on the metagenes (Figure 3). Whereas the fold change values for the rescued mRNAs are contained between 0 for the *rrp47Δ* strain and around -2 for the wild-type, the log<sub>2</sub> fold changes for the ncRNAs are all positive spanning between 0.1 for the wild-type and 0.5 for the deletion strain. These results suggest that the perturbation of the transcriptome by Rho activity leads to a stabilization of ncRNAs either directly or indirectly. As expected, this RNA stabilization is further increased upon depletion of the exonuclease Rrp6 in the *rrp47Δ* strain.

A visual inspection of the reads coverage in a 100 bp window flanking the annotated termination sites indicated that, in addition to the general increase of the reads signals, Rho induces also termination defects of the ncRNAs. The presence of extended transcripts arising from termination defects is more obvious when analyzing independently transcribed snoRNA genomic features, although the presence of such transcript extensions could also be seen for some isolated CUTs and SUTs (Figure 4A and Figure S5). Note, however, that the scales of the reads counts in Figure 4A and Figure S5 differ between the wild-type and the *rrp47Δ* strain for each ncRNA category, reflecting the substantial additional stabilization of these RNAs upon depletion of Rrp6. To have a global view of the Rho-induced termination defects on all the studied RNAs, we plotted the normalized reads counts in the 100 bp region downstream from each annotated transcription unit obtained for the wild-type strain in the absence of Rho versus the same measure obtained in the presence of Rho (Figure 4B). The threshold for a significance of termination read-through was set as log<sub>2</sub> fold change  $\geq 1$  (dotted line) and with p-values below 0.05. The plot revealed that the termination of mRNAs was barely affected by Rho (only 5% of the transcripts above the cut-off), whereas the termination defects were observed for 56% of snoRNAs, 35% of CUTs and 50% of SUTs.

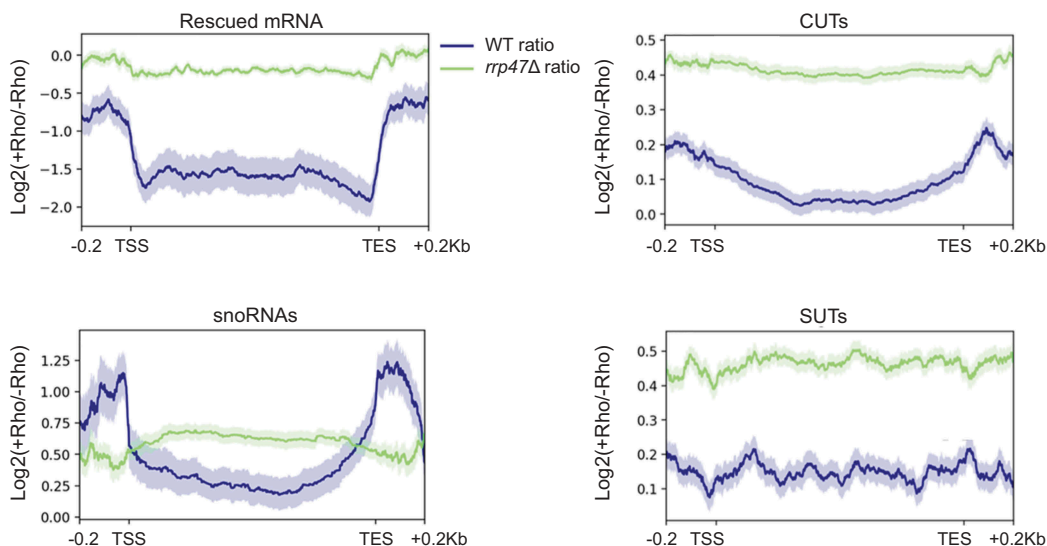


**Figure 3.** Differential effect of Rho on mRNAs and ncRNAs. The Log<sub>2</sub> ratios of RNA levels between +Rho and -Rho conditions are plotted on the metagenes for each RNA biotype as indicated on the top of each graph. Blue lines are for RNAs extracted from Wt cells and green lines are for RNAs obtained from the *rrp47Δ* strain. Standard error is represented by the lightened area around each line.



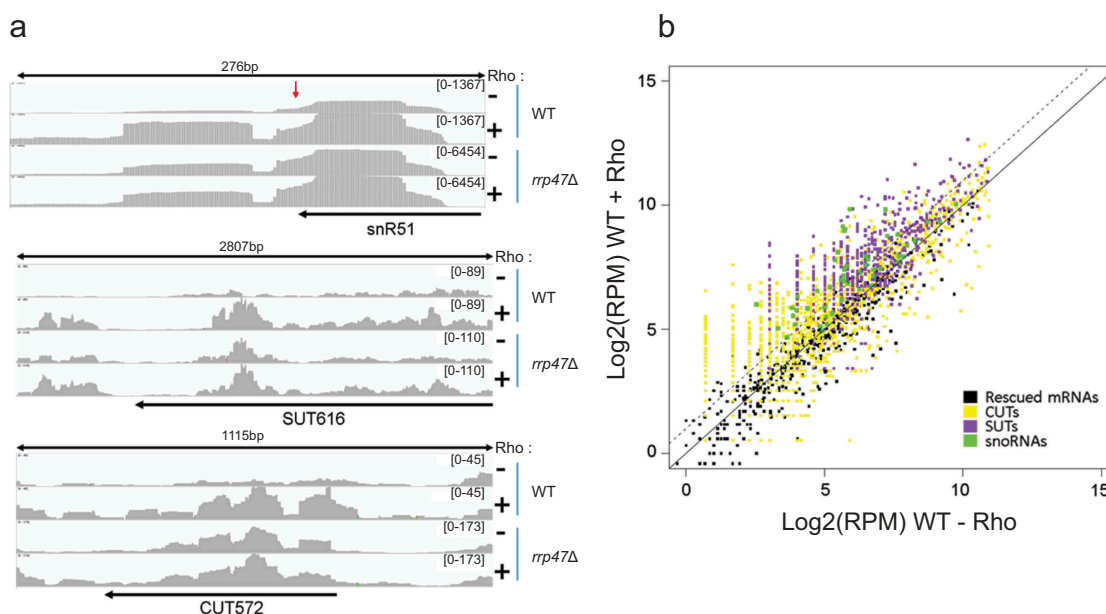


**Figure 4.** Rho activity in yeast affects the termination and processing of ncRNAs. **a)** IGV snapshots of raw RNA-seq reads focusing on a snoRNA, a SUT and a CUT. Each snapshot shows the reads coverage of RNAs extracted from WT or *rrp47Δ* strains and with or without Rho induction. The scale for the number of reads obtained from the raw RNA-seq data is shown in brackets on the right of each snapshot. Red arrow for snR51 indicates the annotated termination site for the snoRNA. **b)** Scatter plot of  $\text{Log}_2$  normalized reads counts in a 100 bp region downstream of annotated genomic features for RNAs extracted from WT cells under Rho perturbation versus the same measure for RNAs obtained from unperturbed cells. Dashed line shows the cut-off of  $\text{L2FC} = 1$ . The color code for the analyzed RNA biotypes is inside the graph.

### High-resolution mapping of Rrp6-dependent QC components association with chromatin

Our previous work on a model mRNA transcript (PMA1) revealed that the co-transcriptional targeting of Rho-induced aberrant mRNPs is mediated by a stimulation of Nrd1 recruitment to the gene locus with a concomitant enrichment by components of the Rrp6-dependent QC. To explore the general nature of the process, we analyzed the genome-wide association with chromatin in - Rho and + Rho conditions of Nrd1, Nab3, Rrp6 and Trf4. Yeast strains harbouring C-terminally tagged proteins expressed from their chromosomal locations under their own promoters were used for chromatin immunoprecipitation followed by single-end deep sequencing (ChIP-seq). The raw data obtained from two independent biological replicates were first verified for their correlation ( $R \geq 0.95$ ) and alignment on the yeast genome. Following this quality examination, the data were used for peak calling by calculating reads ratios between IP and Input in a comparative mode where only peak signals detected simultaneously in the two replicates were considered. The piled-up peak signals obtained for - Rho and + Rho conditions were subsequently subjected to a step of differential analysis where only peaks appearing for one condition but not for the other were scored [22]. This differential ChIP-seq analysis is more appropriate to determine differences between conditions when analyzing large populations of peaks. The processed data for the genomic features of the 491 mRNAs that were affected by Rho and rescued upon Rrp6 depletion are presented as a Beeswarm plot in Figure 5A. The results reveal a strong Rho-mediated stimulation of Nrd1 and Nab3 recruitment to the genes, with 91% of the genes showing at least one peak for Nrd1 and 39% for Nab3. Moreover, the scoring results show also a higher level of occupancy by the two proteins in the

presence of Rho. The Rho-induced large enrichment to chromatin within the Rho-affected genes is also clearly seen for Rrp6 and Trf4 with 45% and 82% of the genes showing at least one peak, respectively.

These ChIP-seq results indicate that the Rrp6-dependent QC components are involved physically in the recognition and targeting of aberrant mRNPs at the co-transcriptional level. Indeed, close visual examinations of individual genomic loci, as shown by representative examples in Figure 5C and Figure S6, highlight the Rho-mediated stimulation of QC recruitment to chromatin. The landscape of Nrd1 association with chromatin reveals broad occupancy profiles that cover the whole body of the affected genes. This underlines the known coupling of Nrd1 with transcribing RNAP II following its recruitment by the CTD (see discussion). Alternatively, the occupancy profiles for Nab3, Rrp6 and Trf4 display rather sharp peaks with significant cross-overlapping, suggesting a possible co-localization of the QC components over portions of the Rho-affected genes. To elucidate a potential spatial correlation between the occupancy sites for the four proteins, we conducted a global analysis of the peaks distributions over the 491 Rho-affected mRNA genes. We used the *genometricorr* package to assess the Empirical Distribution Cumulative Function (ECDF) correlations and evaluated the uniformity of the distributions with the Kolmogorov-Smirnov test. The pair-wise comparisons of the peak signals for the four ChIPed proteins revealed that their relative distributions deviate from independence (Figure S7). Moreover, the averaged relative distances between the peaks of protein pairs over the analyzed genomic loci showed significant positive correlation under Rho expressing conditions compared to repressing conditions (Figure 5B). This suggests a close spatial localization of the QC proteins within chromatin upon co-transcriptional recognition and targeting of the aberrant mRNPs.

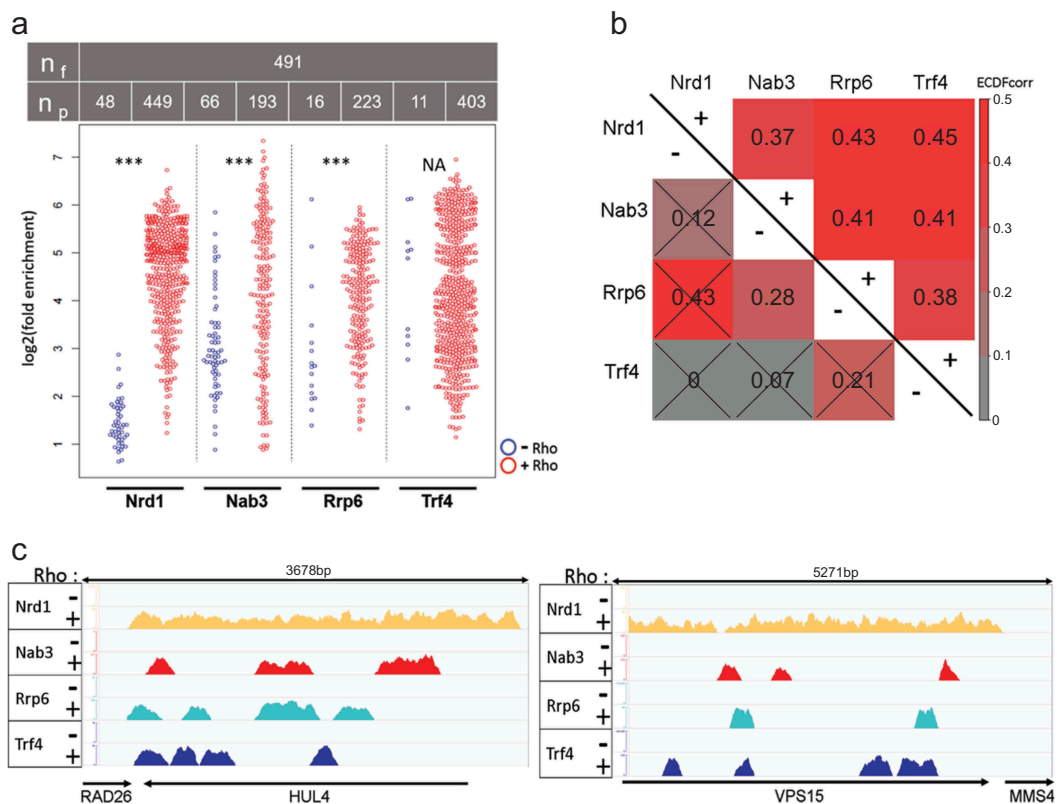


**Figure 5.** Rho activity mediates the stimulation of massive recruitment of QC components to Rrp6-sensitive mRNAs genomic loci. **a)** Beeswarm plot of  $\log_2$  fold enrichment detected on the rescued mRNAs genomic loci obtained by ChIP-seq experiments for each indicated QC protein. The ChIP signals are shown as open dots in blue for -Rho and in red for +Rho conditions. A student t-test was used to assess the significance of enrichment differences between the -Rho and +Rho conditions with the following code 0.05>\*.01>\*\*.001>\*\*\*. (NA) stands for not applicable. The table above the graphs gives the number of analysed features ( $n_f$ ) and the number of loci possessing at least one peak for each protein ( $n_p$ ) in -Rho or +Rho conditions. **b)** Correlogram of Empirical Distribution Cumulative Function correlation area (calculated with the *geometricorr* package) for each protein pairs over the analysed genomic loci under Rho perturbation (“+” symbols) or not (“-” symbols). The crossed boxes indicate the absence of correlation significance. **c)** IGV snapshots of ChIP-seq peaks mapped over two rescued mRNAs genomic loci. The ChIP signals for each protein are shown both for -Rho and +Rho conditions.

### Rho-mediated ncRNAs processing and termination defects are linked to loss of Nrd1 and Nab3 recruitment to the genomic features

Previous studies have reported that nuclear depletion of Nrd1 by the ‘anchor-away’ method gives rise to extended ncRNAs as a result of termination and processing defects [23,24]. In particular, defects in the Nrd1-dependent termination pathway have been shown to induce the extension of snoRNA transcripts into downstream sites similar to our observations described above [23,25–27]. These results led us to consider the possibility that the effect of Rho on processing and termination of ncRNAs may stem somehow from a specific depletion of Nrd1 within these genomic loci. To explore this hypothesis, we extended our ChIP-seq data processing to ncRNAs genomic features. The distribution of the ChIP-seq signals detected over the analyzed ncRNAs genomic loci are presented as Beeswarm plots with the CUTs and SUTs pooled together (Figure 6A) and snoRNAs depicted alone (Figure 6B). In the absence of Rho, Nrd1 enrichment signals were detected over 67% of the CUTs + SUTs and 87% of the snoRNA genomic loci. Some of the enrichment signals, in particular, those over the snoRNAs, are relatively strong. A similar trend was observed for the ChIP-seq analysis obtained with Nab3, supporting the known close association of the two proteins at the ncRNAs termination sites. Remarkably, the presence of Rho leads to a drastic decrease of both the number of Nrd1 and Nab3 peaks detected as well as their

intensity over the CUTs and SUTs, albeit the decrease in the intensity of the peaks is less pronounced for Nab3. For the snoRNAs loci, however, the action of Rho seems to differ somewhat leading to a significant decrease of the enrichment intensity for Nrd1 but only a slight reduction in the number of peaks detected (Figure 6B). Additional analyses showed that the QC components (Rrp6 and Trf4) are also recruited to ncRNAs loci (Figure 6A and B). For Rrp6, however, the intensity of the peak signals is relatively low and does not change significantly between -Rho and +Rho conditions. In contrast, Rho activity appears to stimulate the recruitment of Trf4 to ncRNAs loci in a similar way than for the Rho-affected mRNA genes.

These results together with those of the RNA-seq analysis described above substantiate the known key role of Nrd1 and its partner Nab3 in the termination and processing of ncRNAs. Moreover, the data highlight a link between Rho activity in yeast and a remodelling of the Nrd1-dependent termination machinery within the ncRNAs genomic features leading to transcriptional read-through. To monitor the interplay between the loss of QC proteins from ncRNAs loci and their enrichment within mRNA genes as a result of Rho action, we sought to visualize the protein distributions over the whole genome. This global view was obtained using the Omic Circos software package that generates a circular layout of the 16 yeast chromosomes wreathed with the ChIP-seq peaks detected for the four proteins (Figure 7).

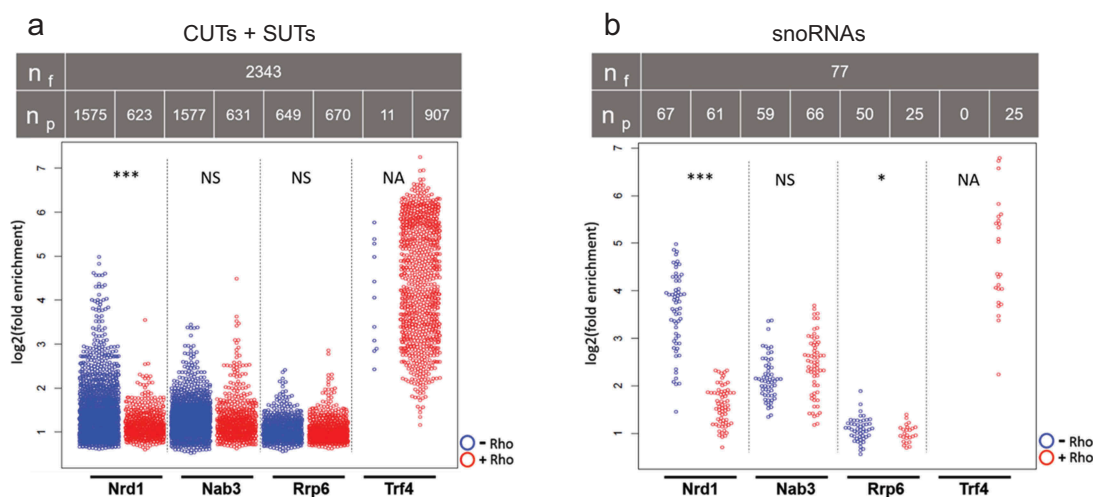


**Figure 6.** Eviction of QC components from ncRNAs genomic features under conditions of perturbation of mRNPs biogenesis by Rho. Beeswarm plots of log<sub>2</sub> fold enrichment obtained by ChIP-seq experiments for each indicated QC protein detected on CUTs and SUTs in (A) and on snoRNAs genomic loci in (B). The symbols and labelling are the same as in Figure 5A. (NS) stands for non-significant according to the Student t-test which is related to the difference in the intensity of the peaks. (NA) stands for not applicable owing to the lack of a significant number of peaks in the -Rho condition.

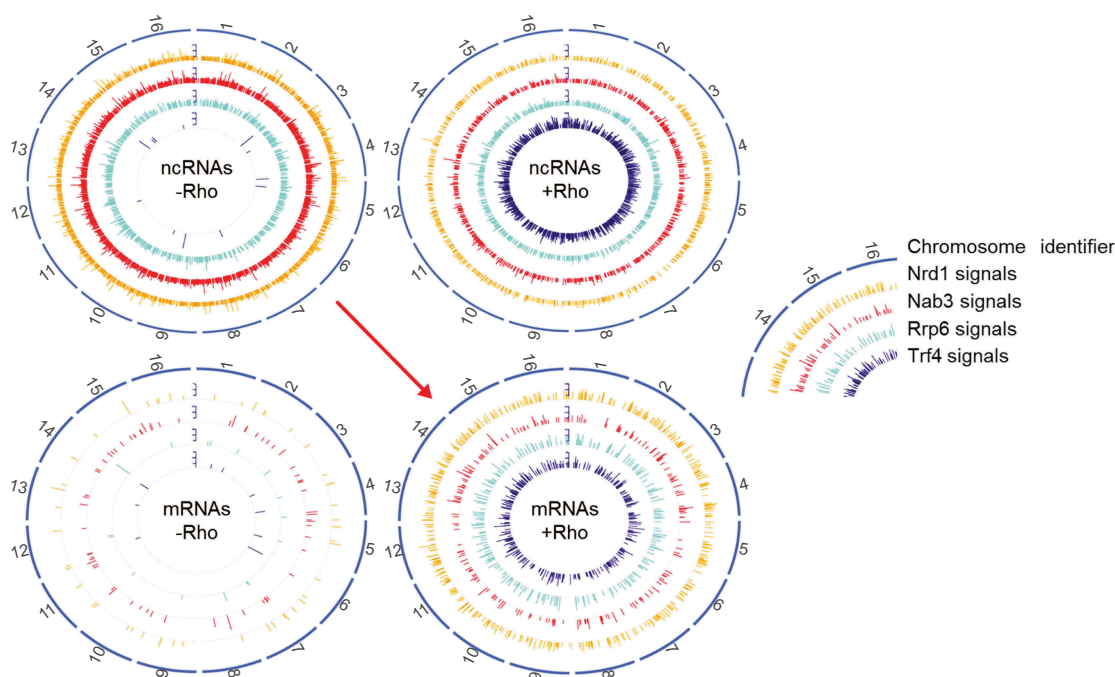


**Figure 7.** Summary of the observed dynamic landscape of QC components over the yeast genome. Circos plots summarising the ChIP-seq results for the four QC proteins over the 16 yeast chromosomes analysed under -Rho (left plots) and +Rho (right plots) conditions. The two top plots show the ChIP signals detected for the ncRNAs genomic loci (CUTs, SUTs and snoRNAs). The two plots at the bottom show the ChIP signals detected for the genomic features of the Rho-affected mRNAs that were rescued by Rrp6 depletion. The red arrow symbolizes the hijacking of Nrd1 and Nab3 from ncRNAs genomic loci to the Rho-affected mRNA genes upon perturbation of mRNP biogenesis by Rho.

Comparisons between the plots obtained for the ncRNAs and Rho-affected mRNAs under -Rho and +Rho conditions show clearly a wide shift reminiscent of a migration of Nrd1 and Nab3 from ncRNAs genomic positions to mRNA genes in the presence of Rho. This suggests that Nrd1 and Nab3 are probably titrated-out from ncRNAs genomic features by their attachment to Rho-affected mRNA genes, generating extended ncRNAs. In contrast, it appears that the Rho-induced stimulation of Rrp6 recruitment to mRNA genes does not depopulate significantly its presence within ncRNAs loci. The plots show also the large recruitment of

Trf4 to both ncRNAs and mRNA genomic features in the presence of Rho, substantiating the role of the TRAMP complex in the targeting of aberrant mRNPs as well as extended ncRNAs [28].

## Discussion

Current views of nuclear mRNP QC mechanism suggest that aberrant mRNPs with processing and packaging defects are targeted co-transcriptionally by the surveillance system triggering their eventual degradation by the catalytic activity of the 3'-5'

exonuclease Rrp6. However, this assumption is based mostly on the observation that defective mRNPs made in yeast mutants with packaging and export flaws are retained within their site of transcription prior to their elimination [7,29,30]. Thus, it is still unclear how the surveillance system is precisely coordinated both physically and functionally with the transcription machinery to detect the faulty events that may arise at each step of the mRNP formation. By implementing an experimental approach in which bacterial Rho factor disturbs mRNP biogenesis in yeast (reviewed in [10]), we conducted a genome-wide examination of mRNPs that are affected by Rho during their formation leading to their targeting by the QC system. This global analysis of the fate of defective mRNPs was accompanied with high-resolution mapping of Rrp6-dependent QC components association with chromatin. The study provides an integrated view of how the activation of the surveillance system displaces the QC components from their regular functional locations within termination sites of ncRNAs genomic loci to populate Rho-affected mRNA genes and target co-transcriptionally the defective mRNPs.

Our RNA-seq analysis identified 1,015 mRNAs that were affected by Rho activity leading to a QC-mediated reduction in their steady-state levels. However, we focused our present study on the 491 transcripts whose targeting was found to be mediated by the Rrp6-dependent QC (Figure 2). This group of transcripts showed a relatively lower level of overall expression in the absence of Rho perturbation as revealed by the comparison between their averaged meta-transcript profile and the averaged profile obtained with the remaining pool of 524 transcripts that we expect to be targeted by the alternative Rat1-dependent QC pathway [18 and manuscript in preparation]. Thus, there is clearly a difference at the transcriptional level that distinguishes the two pools of transcripts.

An interesting feature for the pool of 491 transcripts targeted by the Rrp6-dependent QC is the presence of a comparatively higher reads density within the 5'end region of the averaged meta-transcript profile. This enrichment of transcripts at the 5'end of the genes may indicate the presence of a significant population of paused transcription complexes and/or premature termination as previously revealed by the NET-seq analysis [31] and supported by a more recent study using the RNA cross-linking (CRAC) method [32]. We note, however, that the peak of RNA reads at the 5'end of the averaged profile is probably accentuated in our case by the filtering of the 491 transcripts based on their susceptibility to the Rrp6-dependent QC following Rho action. Obviously, this is an indication for a common feature shared by the selected subset of genes such as a higher level of Ser5 phosphorylation of the CTD of RNAP II within the promoter-proximal pausing region that was also seen in the CRAC study [32]. Interestingly, the Nrd1 component of the Nrd1-Nab3-Sen1 (NNS) complex, involved in termination, processing and decay of ncRNAs, binds preferentially to Ser5 phosphorylated CTD of RNAP II via its CTD-interacting domain (CID) [33,34]. Nrd1 interacts also with RNA by recognizing sequence elements in the nascent transcript in association with Nab3 [35,36]. The recent genome-wide studies of RNA-protein cross-linking in yeast have shown that, in addition to their implication in the metabolism of ncRNAs, Nrd1 and Nab3 play also an important role in the regulation of many mRNA coding genes by remodelling gene expression during nutritional shift or during a stress-response

process [28,37–39]. For instance, the study by Bresson et al. [28] revealed that upon glucose withdrawal, growth-related genes showed reduced expression with a concomitant increase of Nab3 binding to the transcripts, suggesting that this subset of mRNAs represent specific targets for the NNS.

Our previous studies on two model genes (*PMA1* and *PGK1*) have shown that the targeting and elimination of Rho-induced aberrant mRNPs are mediated by a stimulation of Nrd1 co-transcriptional recruitment to the genes. The results led us to suggest that this recruitment may promote the attachment of Rrp6-dependent QC components to the nascent transcript affected by Rho action [11,13]. Our present ChIP-seq data provide a strong support to this suggestion by revealing a combined association of Nrd1, Nab3, Rrp6 and Trf4 to chromatin within a large collection of Rho-affected genes (Figure 5 and Figure S6). The ChIP profiles reveal a broad occupancy of Nrd1 that covers the whole gene locus reflecting its association with RNAP II while transcribing along the gene. Alternatively, the ChIP profiles of the Nrd1 partner, Nab3, show rather relatively sharp and discrete peaks within the body of the genes. These profiles agree with previous RNA-protein cross-linking results indicating broad peak clusters for Nrd1 and isolated peaks for Nab3 [37]. The ChIP-seq profiles of Rrp6 and Trf4 show also relatively sharp and discrete peaks within the body of the genes with statistically significant co-localization of the occupancy regions that also overlap with Nab3 peaks (Figure 5 and Figure S6). Together, these chromatin association profiles suggest that the targeting of Rho-induced aberrant mRNPs by the Rrp6-dependent QC relies on the co-transcriptional recruitment and stabilization of a complex made by Nrd1 and Nab3. In our view, Nrd1 might be weakly anchored to the transcription complex through the interaction of its CID with the CTD of RNAP II within the promoter-proximal part of the gene, a process that could be more common for a subset of genes such as the pool of 491 genes studied here. This primary interaction of Nrd1 is stabilized further by binding in association with Nab3 to specific RNA segments uncovered by Rho action, a fact that mimics a faulty event in mRNP packaging. The importance of the Nrd1-Nab3 association in this early step of the targeting process is also inferred from our previous studies with model genes. In effect, we showed that the targeting of aberrant mRNPs as well as the growth defect phenotype induced by Rho were suppressed when the Nrd1 and Nab3 coupling was flawed by a specific mutation in the Nab3 RNA-binding domain (*nab3-11* allele in [11]) or a deletion of the Nab3-association domain within Nrd1 (*nrd1ΔNID* in [18] and in Figure S8). Thus, the formation of the Nrd1-Nab3 dimer and its stabilization by RNA binding play a key role in the recognition and targeting of aberrant mRNPs.

The statistically relevant co-localization of the four cross-linked proteins within discrete regions of the chromatin indicates that they are part of the same complex as suggested by others [40,41]. Indeed, previous immunoprecipitation studies have detected a physical interaction between Nrd1 and Rrp6, although the precise interacting domains within the proteins are still unknown [20]. More recently, Trf4 was shown to interact physically and functionally with the CID of Nrd1 in a mutually exclusive manner regarding the CTD of transcribing RNAP II



[41,42]. Thus, the stabilization of the Nrd1-Nab3 dimer by RNA binding at the first step of the targeting of aberrant mRNPs should liberate the CID from the CTD allowing the tethering of Rrp6 as well as the TRAMP complex via Trf4 interaction. The formation of such appended complex may constitute a second step of the QC process at which the mRNP is labelled as aberrant. Subsequently, upon transcription completion and the freeing of the transcript 3' end, the labelled mRNP would be prevented from export and directed for destruction either by the direct action of Rrp6 alone as was suggested previously [43,44] or following a coupling of Rrp6 with the exosome.

According to the recent and probably more accurate protein copy-number estimations [45], the number of Nrd1 and Nab3 molecules per yeast cell are of similar magnitude (1,916 and 1,723, respectively). Remarkably, our ChIP-seq results reveal the binding landscape of the two NNS components over the yeast genome with nearly all the molecules localized within ncRNAs genomic loci in the absence of Rho perturbation. In effect, as revealed in Figure 6 A and B, the number of features having at least one peak for Nrd1 (1575 for CUTs +SUTs and 67 for snoRNAs) and the number of features having at least one peak for Nab3 (1577 for CUTs +SUTs and 59 for snoRNAs) are close to the number of molecules per cell. The perturbation of mRNP biogenesis by Rho action appears to disturb this distribution by titrating the two components of the termination and processing complex from their genomic locations. This hijacking of the two NNS components by Rho-affected mRNA genes generates read-through transcripts of ncRNAs as revealed by our RNA-seq results. Also, the Rho-induced large recruitment of Trf4 to the ncRNAs genomic features is a real signature that extended read-through transcripts generated by the local lack of Nrd1 and Nab3 are being discarded following polyadenylation by the TRAMP complex as previously observed following total nuclear depletion of the NNS components [23,24,46,47]. Together, these results provide a global view of the subtle balance of the NNS components within the yeast cell that can be readily perturbed upon a nutritional shift or by stress-induced factors such as bacterial Rho in our experimental approach.

## Materials and methods

### Yeast strains and plasmids

All the *S. cerevisiae* yeast strains used in this study are derived from the wild-type strain BMA41 (*MATa* or *MATα ade2-1 ura3-1 leu2-3,112 his3-11,15 trp1Δ can1-100*) [48]. They have been previously described [11,13,18] except *NRD1-MYC* and *NAB3-MYC* which were newly created. To construct these new strains expressing C-terminally MYC-tagged Nrd1 or Nab3 proteins, PCR products were amplified with the forward and reverse primers (listed in Table S1) on plasmid template pYM19 [49] and integrated into the *NRD1* locus or the *NAB3* locus by homologous recombination. Selected transformants were analyzed by PCR amplification and sequencing of the PCR products then immunoblotting was used to verify the presence of the tag.

*S. cerevisiae* cells were grown according to standard procedures at 25°C in synthetic complete medium with bases and amino acids

omitted as necessary for selection and with glucose (2%) as a carbon source. The cell growth was monitored by measuring the optical density at 600 nm. The pCM185 vector (CEN, TRP1) from Euroscarf was used as a backbone to create the Doxycycline-regulated (Tet off) Rho expression construct (pCM185-Rho-NLS) which was described previously [12]. Strains transformed by Rho expression vector were grown under repressing conditions (5 µg/mL of Doxycycline) at 25°C in YNB medium supplemented with SC-TRP (Synthetic Complete Supplement Mixture from MP Biomedicals) and glucose as carbon source (final concentration 2%). To allow the expression of Rho, the yeast cells were grown in the same medium but without Doxycycline. Growth was performed during 16-hours incubation at 25°C.

### RNA extraction and high-throughput sequencing

Total RNA extraction was performed using the acidic hot phenol/chloroform method as previously described [12]. Quantification of the 18S transcript or the randomly picked transcripts by reverse transcription coupled to semi-quantitative or real-time quantitative PCR was done using Maxima First strand cDNA synthesis Kit from Thermo Scientific and specific oligonucleotides (described in supplementary Table 2). Libraries preparations were made by I2BC high-throughput sequencing platform (Gif sur Yvette) using Illumina ScriptSeq protocol after RiboZero treatment. All samples were processed in duplicates.

### Chromatin immunoprecipitation (ChIP) and NGS libraries preparation

ChIP was performed as described previously [11,13] with some modifications. Following cross-linking and sonication of cell lysates in 1.2 mL of FA140 buffer (50 mM Hepes pH 7.5, 140 mM NaCl, 1 mM EDTA, 1% Triton X-100, 0.1% Sodium deoxycholate and 1:100 Protease Inhibitor Cocktail from Promega), the samples were centrifuged at 2500 g and the supernatant recovered. Twenty microlitres of supernatant genomic DNA was used as Input and the remaining was mixed with antibody solution (anti-c-MYC sc-40X from Santa Cruz Biotechnology). Tubes were incubated overnight at 4°C, then protein G PLUS-agarose beads (Sigma) were added and rotated for 2 hours at 4°C followed by successive washing steps: 2 times with FA140 lysis buffer, 2 times with FA360 lysis buffer (similar to FA140 but with 360 mM NaCl instead of 140 mM), 1 time with washing buffer and 1 time with TE. DNA was eluted twice at 65°C in elution buffer during 10 minutes. Samples (regardless of Input or IP) were reverse cross-linked at 65°C overnight. Proteinase K digestion of the eluates was performed prior to purification of the genomic DNA samples using the ThermoFisher GeneJET PCR Purification Kit.

ChIP libraries preparation was performed following the NEBNext Ultra II DNA Library Prep instructions from New England Biolabs. All ChIP libraries samples were made in duplicates. The sequencing was performed by I2BC high-throughput sequencing platform (Gif sur Yvette) using Illumina ScriptSeq protocol.

### Data processing and computational analysis

RNA-seq reads were quality controlled (using FastQC v 0.11.5), the adapters were trimmed using Cutadapt 1.15, and then reads were uniquely aligned to *Saccharomyces cerevisiae* genome V64.1.1 (downloaded from SGD) with bwa 0.7.12 (bwa mem - T 30 - t 6) with default settings except for the minimal quality. Samtools 0.1.19 was used to assess the alignment quality. Reads per genes were counted with featureCounts V 1.5.0-p1 (from the subreads suite) with the strand-specific option (-s 1). The genome annotations were downloaded from SGD and ncRNAs annotations were taken from Xu et al. [21] for SUTs and from Neil et al. [19] for CUTs.

Differential expression analyses were performed under the R environment (V 3.4.4) using DESeq2 package. For each genetic background (WT or *rrp47Δ*) duplicates from Rho-induced conditions (+Rho) were compared to duplicates from Rho repressed conditions (-Rho). The statistically down-regulated genes (p-value < 0.05 and L2FC < -0.5) from WT background in +Rho conditions (1,015 mRNAs) were isolated and their compartments were analyzed in the mutant conditions (491 were rescued). BigWig files were generated as following using bedtools V2.25.0 (genomcov and bigwigCompare), and UCSC tool bedGraphToBigWig. After computing genome coverage (with genomcov), bedgraph outputs were converted to bigwig files using bedGraphToBigWig. Meta-profiles plots were made using bedtools V2.25.0 with computeMatrix (scale-regions mode, with a bin size of 1 base) on BigWig files and plotProfile for graphical output.

ChIP-seq reads were submitted to the same processing steps than RNA-seq reads except for the strand specificity. Peak calling was performed using PePr V1.1.21 [50] which was chosen because it allows performing analysis of duplicates directly and in a comparative mode when needed. Differential peak calling was used for focusing on mRNAs loci enriched in +Rho condition compare to -Rho condition. Classical peak calling was used to analyse the other RNAs biotypes loci. Manipulations on peak caller outputs were done mostly with R. Figures were built with a ggplot2 package and Circos plots were done using OmicCircos package. Plots of the distributions of peaks signals by RNA biotypes loci and by proteins were made using Beeswarm package.

### Statistical analyses

Spearman correlation test was used to control the correlation between biological replicates. Student t-test (bidirectional) was used to compare levels of L2FC between RNA-seq conditions and between -Rho and +Rho ChIP-seq Log2(average signals). NS > 0.05 > \* > 0.01 > \*\* > 0.001 > \*\*\*. Jaccard and permutations tests were done using the genomcorr package in order to determine if the distribution of peaks of two 'ChIPed' proteins on the yeast genome overlap significantly (not due to hazard).

### Visualization

All snapshots used for direct visualization of reads coverage or ChIP peaks distributions were taken with IGV browser.

### Accession numbers for deposited sequencing data at array express database

RNA-seq: E-MTAB-7538

For reviewer access, please use the following username and password

Username: Reviewer\_E-MTAB-7538

Password: A8Vhdeky

ChIP-seq: E-MTAB-7539

For reviewer access, please use the following username and password

Username: Reviewer\_E-MTAB-7539

Password: vvyFH5np

### Acknowledgments

This work was supported by the CNRS recurrent funding and has been sponsored in part by support from Région Centre-Val de Loire through research grants (Anti-Rho-Biotics, and ARD2020 Biomédicaments) to A. R. Rahmouni. K. Moreau was a recipient of a PhD fellowship from the Région Centre-Val de Loire. The genome-wide analyses have benefited from the processing workflow and expertise of the High-throughput Sequencing Platform of I2BC, CNRS Gif sur Yvette.

### Disclosure statement

No potential conflict of interest was reported by the authors.

### Funding

This work was supported by the Conseil Régional du Centre-Val de Loire [Ph.D fellowship]; Conseil Régional du Centre-Val de Loire [Anti-Rho-Biotics].

### ORCID

Kévin Moreau  <http://orcid.org/0000-0002-3686-0737>

Aurélia Le Dantec  <http://orcid.org/0000-0002-7293-4481>

Yves Bigot  <http://orcid.org/0000-0001-9476-0710>

### References

- [1] Bentley DL. Coupling mRNA processing with transcription in time and space. *Nat Rev Genet.* 2014;15:163–175.
- [2] Luna R, Gaillard H, Gonzalez-Aguilera C, et al. Biogenesis of mRNPs: integrating different processes in the eukaryotic nucleus. *Chromosoma.* 2008;117:319–331.
- [3] Doma MK, Parker R. RNA quality control in eukaryotes. *Cell.* 2007;131:660–668.
- [4] Fasken MB, Corbett AH. Process or perish: quality control in mRNA biogenesis. *Nat Struct Mol Biol.* 2005;12:482–488.
- [5] Schmid M, Jensen TH. Transcription-associated quality control of mRNP. *Biochim Biophys Acta.* 2013;1829:158–168.
- [6] Singh P, Saha U, Paira S, et al. Nuclear mRNA surveillance mechanisms: function and links to human disease. *J Mol Biol.* 2018;430:1993–2013.
- [7] Rougemaille M, Gudipati RK, Olesen JR, et al. Dissecting mechanisms of nuclear mRNA surveillance in THO/sub2 complex mutants. *Embo J.* 2007;26:2317–2326.
- [8] Schmid M, Jensen TH. Quality control of mRNP in the nucleus. *Chromosoma.* 2008;117:419–429.
- [9] Villa T, Rougemaille M, Libri D. Nuclear quality control of RNA polymerase II ribonucleoproteins in yeast: tilting the balance to shape the transcriptome. *Biochim Biophys Acta.* 2008;1779:524–531.

- [10] Mosrin-Huaman C, Hervouet-Coste N, Le Dantec A, et al. Bacterial Rho helicase: a new tool to dissect mRNP biogenesis and quality control in yeast. *Trends Cell Mol Biol.* 2014;9:79–93.
- [11] Honorine R, Mosrin-Huaman C, Hervouet-Coste N, et al. Nuclear mRNA quality control in yeast is mediated by Nrd1 co-transcriptional recruitment, as revealed by the targeting of Rho-induced aberrant transcripts. *Nucleic Acids Res.* 2011;39:2809–2820.
- [12] Mosrin-Huaman C, Honorine R, Rahmouni AR. Expression of bacterial Rho factor in yeast identifies new factors involved in the functional interplay between transcription and mRNP biogenesis. *Mol Cell Biol.* 2009;29:4033–4044.
- [13] Stuparevic I, Mosrin-Huaman C, Hervouet-Coste N, et al. Cotranscriptional recruitment of RNA exosome cofactors Rrp47p and Mpp6p and two distinct Trf-Air-Mtr4 polyadenylation (TRAMP) complexes assists the exonuclease Rrp6p in the targeting and degradation of an aberrant messenger ribonucleoprotein particle (mRNP) in yeast. *J Biol Chem.* 2013;288:31816–31829.
- [14] Feigenbutz M, Garland W, Turner M, et al. The Exosome cofactor Rrp47 is critical for the stability and normal expression of its associated exoribonuclease Rrp6 in *Saccharomyces cerevisiae*. *PLOS ONE.* 2013;8:e80752.
- [15] Feigenbutz M, Jones R, Besong TM, et al. Assembly of the yeast exoribonuclease Rrp6 with its associated cofactor Rrp47 occurs in the nucleus and is critical for the controlled expression of Rrp47. *J Biol Chem.* 2013;288:15959–15970.
- [16] Schuch B, Feigenbutz M, Makino DL, et al. The exosome-binding factors Rrp6 and Rrp47 form a composite surface for recruiting the Mtr4 helicase. *Embo J.* 2014;33:2829–2846.
- [17] Lang WH, Platt T, Reeder RH. *Escherichia coli* rho factor induces release of yeast RNA polymerase II but not polymerase I or III. *Proc Natl Acad Sci U S A.* 1998;95:4900–4905.
- [18] Mosrin-Huaman C, Hervouet-Coste N, Rahmouni AR. Co-transcriptional degradation by the 5'-3' exonuclease Rat1p mediates quality control of HXK1 mRNP biogenesis in *S. cerevisiae*. *RNA Biol.* 2016;13:582–592.
- [19] Neil H, Malabat C, d'Aubenton-Carafa Y, et al. Widespread bidirectional promoters are the major source of cryptic transcripts in yeast. *Nature.* 2009;457:1038.
- [20] Vasiljeva L, Buratowski S. Nrd1 interacts with the nuclear exosome for 3' processing of RNA polymerase II transcripts. *Mol Cell.* 2006;21:239–248.
- [21] Xu Z, Wei W, Gagneur J, et al. Bidirectional promoters generate pervasive transcription in yeast. *Nature.* 2009;457:1033–1037.
- [22] Steinhauser S, Kurzawa N, Eils R, et al. A comprehensive comparison of tools for differential ChIP-seq analysis. *Brief Bioinform.* 2016;17:953–966.
- [23] Schaugency P, Merran J, Corden JL. Genome-wide mapping of yeast rna polymerase II termination. *PLoS Genet.* 2014;10:e1004632.
- [24] Schulz D, Schwalb B, Kiesel A, et al. Transcriptome surveillance by selective termination of noncoding RNA synthesis. *Cell.* 2013;155:1075–1087.
- [25] Steinmetz EJ, Conrad NK, Brow DA, et al. RNA-binding protein Nrd1 directs poly(A)-independent 3'-end formation of RNA polymerase II transcripts. *Nature.* 2001;413:327–331.
- [26] Steinmetz EJ, Ng SB, Cloute JP, et al. cis- and trans-acting determinants of transcription termination by yeast RNA polymerase II. *Mol Cell Biol.* 2006;26:2688–2696.
- [27] Chen X, Poorey K, Carver MN, et al. Transcriptomes of six mutants in the Sen1 pathway reveal combinatorial control of transcription termination across the *Saccharomyces cerevisiae* genome. *PLoS Genet.* 2017;13:e1006863.
- [28] Bresson S, Tuck A, Staneva D, et al. Nuclear RNA decay pathways aid rapid remodeling of gene expression in yeast. *Mol Cell.* 2017;65:787–800.e5.
- [29] Babour A, Shen Q, Dos-Santos J, et al. The chromatin remodeler ISW1 Is a quality control factor that surveys nuclear mRNP biogenesis. *Cell.* 2016;167:1201–14.e15.
- [30] Rougemaille M, Villa T, Gudipati RK, et al. mRNA journey to the cytoplasm: attire required. *Biol Cell.* 2008;100:327–342.
- [31] Churchman LS, Weissman JS. Nascent transcript sequencing visualizes transcription at nucleotide resolution. *Nature.* 2011;469:368–373.
- [32] Milligan L, Huynh-Thu VA, Delan-Forino C, et al. Strand-specific, high-resolution mapping of modified RNA polymerase II. *Mol Syst Biol.* 2016;12.
- [33] Gudipati RK, Villa T, Boulay J, et al. Phosphorylation of the RNA polymerase II C-terminal domain dictates transcription termination choice. *Nat Struct Mol Biol.* 2008;15:786–794.
- [34] Vasiljeva L, Kim M, Mutschler H, et al. The Nrd1-Nab3-Sen1 termination complex interacts with the Ser5-phosphorylated RNA polymerase II C-terminal domain. *Nat Struct Mol Biol.* 2008;15:795–804.
- [35] Conrad NK, Wilson SM, Steinmetz EJ, et al. A yeast heterogeneous nuclear ribonucleoprotein complex associated with RNA polymerase II. *Genetics.* 2000;154:557–571.
- [36] Steinmetz EJ, Brow DA. Control of pre-mRNA accumulation by the essential yeast protein Nrd1 requires high-affinity transcript binding and a domain implicated in RNA polymerase II association. *Proc Natl Acad Sci U S A.* 1998;95:6699–6704.
- [37] Creamer TJ, Darby MM, Jamonnak N, et al. Transcriptome-wide binding sites for components of the *Saccharomyces cerevisiae* non-poly(A) termination pathway: nrd1, Nab3, and Sen1. *PLoS Genet.* 2011;7:e1002329.
- [38] van Nues R, Schweikert G, de Leau E, et al. Kinetic CRAC uncovers a role for Nab3 in determining gene expression profiles during stress. *Nat Commun.* 2017;8:12.
- [39] Webb S, Hector RD, Kudla G, et al. PAR-CLIP data indicate that Nrd1-Nab3-dependent transcription termination regulates expression of hundreds of protein coding genes in yeast. *Genome Biol.* 2014;15:R8.
- [40] Fox MJ, Gao H, Smith-Kinnaman WR, et al. The exosome component Rrp6 is required for RNA polymerase II termination at specific targets of the Nrd1-Nab3 pathway. *PLoS Genet.* 2015;11:e1004999.
- [41] Kim K, Heo D-H, Kim I, et al. Exosome cofactors connect transcription termination to rna processing by guiding terminated transcripts to the appropriate exonuclease within the nuclear exosome. *J Biol Chem.* 2016;291:13229–13242.
- [42] Tudek A, Porrua O, Kabzinski T, et al. Molecular basis for coordinating transcription termination with noncoding RNA degradation. *Mol Cell.* 2014;55:467–481.
- [43] Callahan KP, Butler JS. Evidence for core exosome independent function of the nuclear exoribonuclease Rrp6p. *Nucleic Acids Res.* 2008;36:6645–6655.
- [44] Callahan KP, Butler JS. TRAMP complex enhances RNA degradation by the nuclear exosome component Rrp6. *J Biol Chem.* 2010;285:3540–3547.
- [45] Kulak NA, Pichler G, Paron I, et al. Minimal, encapsulated proteomic-sample processing applied to copy-number estimation in eukaryotic cells. *Nat Methods.* 2014;11:319.
- [46] Grzechnik P, Kufel J. Polyadenylation linked to transcription termination directs the processing of snoRNA precursors in yeast. *Mol Cell.* 2008;32:247–258.
- [47] Jamonnak N, Creamer TJ, Darby MM, et al. Yeast Nrd1, Nab3, and Sen1 transcriptome-wide binding maps suggest multiple roles in post-transcriptional RNA processing. *RNA.* 2011;17:2011–2025.
- [48] Baudin-Baillieu A, Guillemet E, Cullin C, et al. Construction of a yeast strain deleted for the TRP1 promoter and coding region that enhances the efficiency of the polymerase chain reaction-disruption method. *Yeast.* 1997;13:353–356.
- [49] Janke C, Magiera MM, Rathfelder N, et al. A versatile toolbox for PCR-based tagging of yeast genes: new fluorescent proteins, more markers and promoter substitution cassettes. *Yeast.* 2004;21:947–962.
- [50] Zhang Y, Lin YH, Johnson TD, et al. PePr: a peak-calling prioritization pipeline to identify consistent or differential peaks from replicated ChIP-Seq data. *Bioinformatics.* 2014;30:2568–2575.